



# Nanosized tungsten carbide synthesized by a novel route at low temperature for high performance electrocatalysis

Zaoxue Yan<sup>1</sup>, Mei Cai<sup>2</sup> & Pei Kang Shen<sup>1</sup>

<sup>1</sup>State Key Laboratory of Optoelectronic Materials and Technologies, and Key Laboratory of Low-carbon Chemistry & Energy Conservation of Guangdong Province, School of Physics and Engineering, Sun Yat-sen University, 135 Xingang Road, Guangzhou, 510275, PR China, <sup>2</sup>General Motors Research and Development Center, Warren, Michigan, 48090-9055, USA.

SUBJECT AREAS:  
ELECTROCATALYSIS  
FUEL CELLS  
NANOPARTICLES  
CATALYST SYNTHESIS

Received  
1 February 2013

Accepted  
22 March 2013

Published  
10 April 2013

Correspondence and  
requests for materials  
should be addressed to  
P.K.S. (stsspk@mail.  
sysu.edu.cn.)

**Tungsten carbide (WC) is a widely used engineering material which is usually prepared at high temperature. A new mechanism for synthesizing nanoscaled WC at ultralow temperature has been discovered. This discovery opens a novel route to synthesize valuable WC and other carbides at a cost-efficient way. The novel formation mechanism is based on an ion-exchange resin as carbon source to locally anchor the W and Fe species. As an intermediate, FeWO<sub>4</sub> can be formed at lower temperature, which can be directly converted into WC along with the carbonization of resin. The size of WC can be less than 2 nm. The catalyst made with Pt nanoparticles supported on nanosized WC-GC (WC-graphitized carbon) shows enhanced electrocatalytic activity for oxygen reduction reaction. The result also indicates that the Pt nanoparticles deposited on WC-GC are dominated by Pt (111) plane and shows a mass activity of 257.7 mA mg<sup>-1</sup>Pt@0.9 V.**

**T**ungsten carbide (WC) is an interstitial compound of C atoms filling into W crystal, which has high strength and rigidity as covalent compound, high melting point as ionic crystal and electromagnetism as transition metal. WC has wide applications in national defense, chemical industries, electronic industries, mechanical tools and surface coatings<sup>1-6</sup>. WC has the characteristics of high hardness, good wear-resistance, good fracture resistance and high temperature strength. Those properties make it an idea coating material for pottery, china ware, and incise instrument. However, due to the high melting point of WC (normally as high as 2800°C), it is hardly to form horniness alloy through sintering process. Usually, Co metal was used to bind WC particles to improve its bending resistance, but Co reduces the rot-resistance, hardness and wear-resistance of the alloy<sup>1,2</sup>, which caused the development of occupational asthma to a certain degree<sup>7</sup>. Therefore, the methods to sinter WC by discharge of ion<sup>3</sup>, microwave<sup>4</sup>, high frequency inducement<sup>5</sup> and high temperature insostatic pressing<sup>6</sup> were adopted, but the high processing cost restricted their applications in industrial production scale.

The WC nanoparticles as hard metal alloy precursor could obviously improve the strength, hardness and toughness of the sintered alloys<sup>8,9</sup>. The smaller the WC particle size is, the lower the compaction temperature and the shorter the sintering time will be. Goren-Muginstein *et al.* found that nanometer sized WC particles could compact at 500°C, compared to over 1200°C for the micrometer sized WC particles<sup>10</sup>.

Aside from its physical properties, since Levy and Boudar reported the Pt-like performance of WC as catalyst<sup>10</sup>, the research of the WC in chemical and electrochemical catalysis has been widely interested. WC has been proposed to partially or totally replace the noble metals like Pt to reduce the cost<sup>11-26</sup>. WC as catalyst was firstly used for alkane isomerization and showed a high catalytic activity which is comparable with Pt<sup>10,11</sup>. Fairly high catalytic activities were also found for WC in catalyzing hydrogenation of ethane and corn stalk<sup>12-14</sup>, reforming of methane and cellulose<sup>15,16</sup>, decomposition of methanol<sup>17</sup>, dehydrogenation of butane<sup>18</sup>, and hydrogenation and dechlorination of Freon<sup>19</sup> and so on. WC showed the selectivity in catalyzing alkane isomerization and alcohol hydrogenation<sup>20,21</sup> when the surface of WC is being modified or the reaction temperature is being changed. In the electrochemistry, WC alone showed limited activity for oxygen reduction in alkaline solution<sup>22</sup>. Philip *et al.* pointed out that the catalytic activity of WC on hydrogen oxidation was one hundred thousandth of Pt catalyst<sup>23</sup>. But the catalytic activity of WC on methanol oxidation was not so bad<sup>24,25</sup>. Nakazawa *et al.* reported that the electronegative WC could absorb the hydrogen in methanol, leading to the dehydrogenation and oxidation of methanol<sup>26</sup>. Delightfully, the synergistic effect of WC with Pt or Pd has been found in electrocatalysis, that is, WC as electrocatalyst promoter could improve the electrocatalytic activity of noble metal catalyst and could partially



substitute the noble metal<sup>27–31</sup>. Furthermore, WC has higher resistance in acidic solution and higher temperature. It showed a resistance to the CO poisoning, leading to prolonged catalytic life for direct alcohol fuel cells<sup>32–43</sup>.

To prepare WC nanoparticles with cost efficient method, lower energy expenditure, and controllable particle size is a critical challenge for wide application of WC in industries. The traditional synthesis technique for WC involves heating the fully mixed  $\text{WO}_3$  (or W metal) and carbon powder at 1000–1600°C. But the resultant WC particles are generally big in size and lower in specific surface area. Numerous methods have been developed to obtain nanoscale WC particles<sup>44–52</sup>. As an example, less than 10 nm WC particles could be made by ball milling. However this method is time and energy consuming. Moreover, the products produced by ball milling are prone to contamination in milling pot. Shen *et al.* used an improved microwave heating method, the size of the WC particles could be controlled by adjusting the heating and relaxing time<sup>44</sup>. Lee *et al.* exchanged the oxygen in  $\text{WO}_3$  with cation of zeolite halogenate, and then reduced the intermediates to WC by CO at 550–750°C<sup>45</sup>. Due to the difficulty of exchanging the ions in solid materials, the product in general consist of larger WC particles with up to several hundred nanometers in size. Nevertheless, these methods remain more or less the following disadvantages: complex procedures, long time, high temperatures and high energy consumption. Most importantly, it is hardly to obtain pure WC. The products might consist of WC mixed with  $\text{WO}_x$ ,  $\text{W}_2\text{C}$  or  $\text{WC}_{1-x}$  and W metal<sup>53–59</sup>.

Herein, we report the preparation of WC nanoparticles supported on graphitized carbon (WC-GC) with controllable size (1–10 nm) at lower reaction temperatures (550–750°C) and short reaction time (< 1 h) under the aid of additives. It is realized for the first time that the successful yield of pure WC can be achieved at lower temperature. A new synthesis mechanism is therefore proposed.

## Results

Figure 1a–c show the XRD patterns of heat treated resins at 500–900°C which were exchanged in tungsten precursor (WC-GC10, WC-GC5 and WC-GC2) solutions with the presence of  $\text{K}_4[\text{Fe}(\text{CN})_6]$ . It is clear that all the samples have the similar reaction products with changing of temperatures. The  $\text{FeWO}_4$  (XRD: PDF-74-1130) appeared at lower temperatures of 500–600°C. The WC peaks (XRD: PDF-51-0939) appeared at 650°C with  $\text{FeWO}_4$  peaks weakened. Then  $\text{FeWO}_4$  peaks disappeared at 800°C and the peaks of WC became stronger with higher degree of crystallinity at 900°C. What surprised us is that there were no other carbides found but pure WC. The results indicated that WC was formed via an intermediate of  $\text{FeWO}_4$  with the rising of temperature. At the same time, iron acted as a catalyst to graphitize the resin at lower temperature, indicated by the shift of the broad amorphous carbon peak toward the right side and the appearance of graphite peak around 25° in XRD patterns at the temperature over 650°C. The peak of iron carbide appears around 41°.

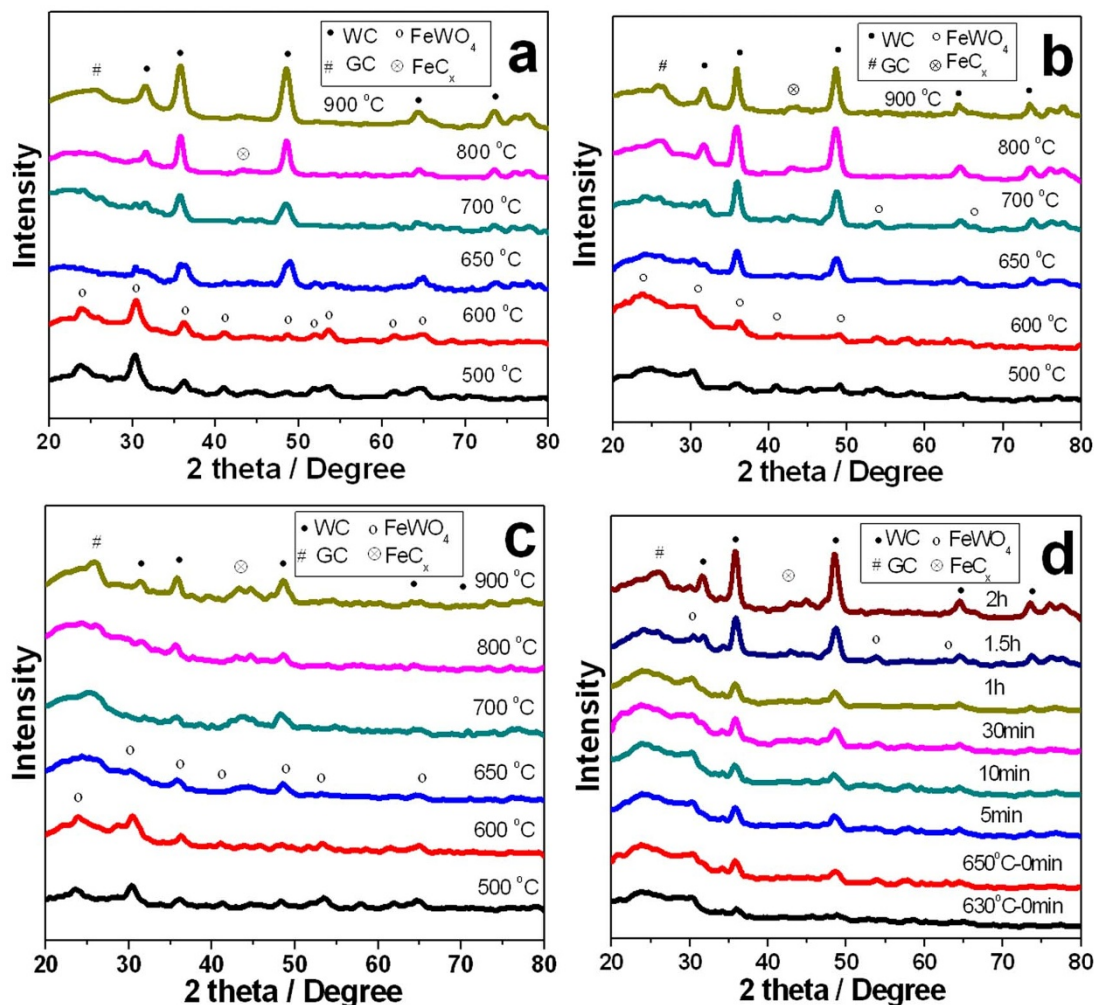


**Figure 1** | XRD patterns of (a) WC-GC10, (b) WC-GC5 and (c) WC-GC2 heated at 500–900°C with the addition of  $\text{K}_4[\text{Fe}(\text{CN})_6]$  and (d) XRD patterns of WC-GC5 at 630–650°C for different times.



The sample synthesized by using D314 resin as carbon source, AMT as W source without  $K_4[Fe(CN)_6]$  is also presented for comparison. Figure 2 shows the XRD patterns. At lower temperatures, tungsten oxide like  $WO_2$  (XRD: PDF-32-1393) dominated the product which was decomposed from  $W_7O_{24}^{6-}$ .  $WC_{1-x}$  (XRD: PDF-20-1316) appeared at  $800^\circ C$ . The final product was a mixture of WC,  $WC_{1-x}$  and  $W_2C$  even after heating at  $1000^\circ C$  for 3 h. It is almost impossible to synthesize pure WC in such conditions.

Figure 3 shows the TEM images of WC-GC10, WC-GC5 and WC-GC2 heated at  $650^\circ C$  for 3 h. It is clear that the WC particles were uniformly dispersed on carbon matrix. Figure 3d is the TEM image of WC-GC5 with lower magnification, while, the inset is the HRTEM image of WC-GC5, the WC (100) and GC (002) crystal lattices can be clearly seen, which further proves the coexistence of WC and partially graphitized carbon in the WC-GC samples. From the randomly selected 100 particles, the average particle sizes were calculated as 5.3 nm, 3.5 nm and 1.9 nm for WC-GC10, C-GC5 and WC-GC2, respectively. The size distribution of the particles was very narrow as shown in Figure 3e, 3f and 3g, indicating the advantages of localized ion exchange.

Pt nanoparticles were further loaded on the WC-GC support to evaluate its oxygen reduction reaction (ORR) activities as an electrocatalyst. Figure 4 compares the XRD patterns of the Pt on WC-GC (denoted as Pt/WC-GC) samples including Pt/WC-GC10, Pt/WC-GC5 and Pt/WC-GC2. The dominating Pt  $2\theta$  peak at  $39.8^\circ$  corresponds to (111) crystal lattice of Pt. The  $2\theta$  peaks at  $46.2^\circ$  and  $67.5^\circ$ , which correspond to (200) and (220) facets of Pt, are hardly discerned. This result suggests that Pt nanoparticles deposited on WC-GC are dominated with Pt (111) plane, which has been approved to be the most active lattice site for oxygen reduction reaction<sup>62</sup>.

Figure S4 shows the TEM images of Pt/WC-GC5. The dispersion of Pt particle is very uniform. The Pt particle size distribution is narrow as shown in the inset of Figure S4a with the average size of 2.0 nm. Figure S4b is the HRTEM image of WC-GC5, in which the graphite crystalline lattice is clearly seen. The inset image also clearly shows the Pt (111) and WC (100) crystal lattices. It is expected that the Pt (111) dominated catalyst will be more active along with the synergistic effect with WC<sup>63</sup> compared with commercial catalyst. Therefore, we further investigated the selective synthesis of Pt (111) nanomaterials onto WC toward ORR.

Figure 5a compares the ORR curves on Pt/WC-GC10, Pt/WC-GC5, Pt/WC-GC2 and commercial Pt/C electrodes in  $O_2$  saturated  $0.1 \text{ mol L}^{-1} \text{ HClO}_4$  solution with a scan rate of  $5 \text{ mV s}^{-1}$  and the rotating rate of 1600 rpm at  $25^\circ C$ . It is clear that the performance of

Pt/WC-GC10, Pt/WC-GC5 and Pt/WC-GC2 were much better relative to the benchmark of Pt/C at 0.9 V. Figure 5b shows the mass activity plots of these electrodes calculated from the experimental data using the well-known mass transport correction for rotating disk electrode<sup>63</sup>:

$$i_k = i_d i / (i_d - i) \quad (1)$$

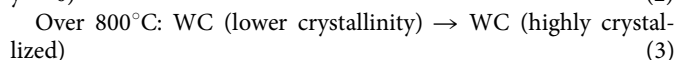
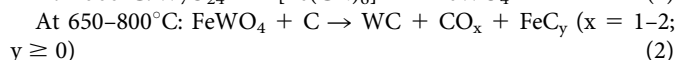
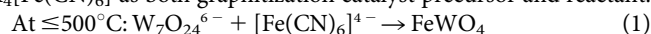
where  $i$  is the experimentally obtained current,  $i_d$  refers to the measured diffusion-limited current and  $i_k$  the mass-transport-free kinetic current. The mass activity can be determined via the calculation of  $i_k$  using equation (1) and normalized with the Pt loadings. The mass activities measured from the curves in Figure 5b are summarized in Table 1. Among the three Pt/WC-GC electrocatalysts, Pt/WC-G5 has the highest catalytic activity for ORR. It is worth to note that in this study, the measured activity of the commercial Pt/C electrocatalyst is in good agreement with the reported or predicted value in literatures<sup>62,63</sup>.

The WC contents in the WC-GC samples are shown in Table 2. The data were obtained through the following process: The WC-GC sample (1 g) was firstly oxidized at  $1400^\circ C$  in air for 1 h to remove all the C elements including amorphous and graphite carbon; then the residue was proved to be pure  $WO_3$  by the characterization of EDS and XRD; at last, the  $WO_3$  powder was weighed and then calculated the WC content in the WC-GC sample. It can be seen from Table 2 that WC-GC2 has too low WC content to fully exert the synergistic effect on Pt. Meanwhile, WC-GC10 has the highest WC content, which certainly has the lowest surface area and could not disperse Pt particles well. However, WC-GC5 has the mediate WC content and surface area comparing to WC-GC2 and WC-GC10, so Pt/WC-GC5 showed the highest catalytic activity.

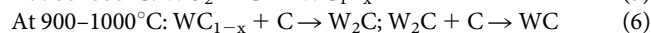
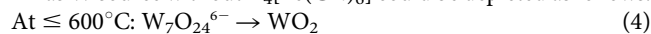
## Discussion

As we know that WC is an interstitial compound with accepted formation mechanism of  $W \rightarrow W_2C$  (or  $WC_x$ )  $\rightarrow$  WC. To deduce the reaction mechanism for our new system, we carefully analyzed the variation of the XRD patterns as the temperatures change. As an example, the WC-GC5 sample with middle ammonium metatungstate (AMT) concentration was selected and heated from room temperature to  $630^\circ C$  and  $650^\circ C$  at a rate of  $5^\circ C \text{ min}^{-1}$ . The sample was then holding at  $650^\circ C$  for 5 min, 10 min, 30 min, 1 h, 1.5 h and 2 h. From the XRD patterns shown in Figure 1d, we can see that the sample consist of single phase  $FeWO_4$  at  $630^\circ C$  without any WC. The WC appeared where the sample was heated to  $650^\circ C$  and hold for 5 min. Continuously heating the sample from 5 min to 1.5 h at  $650^\circ C$  resulted in the peaks of WC became stronger along with the weakening down of the  $FeWO_4$  peaks. The  $FeWO_4$  peaks totally disappeared when the holding time reached 2 h. There were no W metal and other W compounds found in the whole processes, indicating that the WC was converted directly from  $FeWO_4$ .

Based on above results, we propose a reaction mechanism of WC as follows, using resin as carbon source, AMT as W source and  $K_4[Fe(CN)_6]$  as both graphitization catalyst precursor and reactant.



The reaction mechanism of WC using resin as carbon source, AMT as W source without  $K_4[Fe(CN)_6]$  could be depicted as follows.



Since the formation mechanism is different with and without the existence of  $K_4[Fe(CN)_6]$ , pure WC can only be obtained in the presence of  $K_4[Fe(CN)_6]$ .

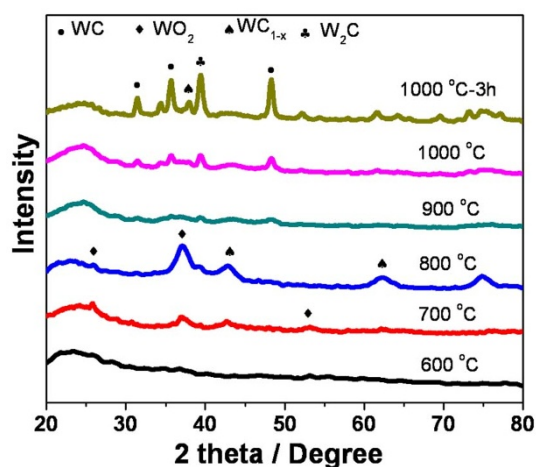


**Figure 2** | XRD patterns of the heat treated D314 resin exchanged in  $0.005 \text{ mol L}^{-1}$  W precursors without  $K_4[Fe(CN)_6]$ .

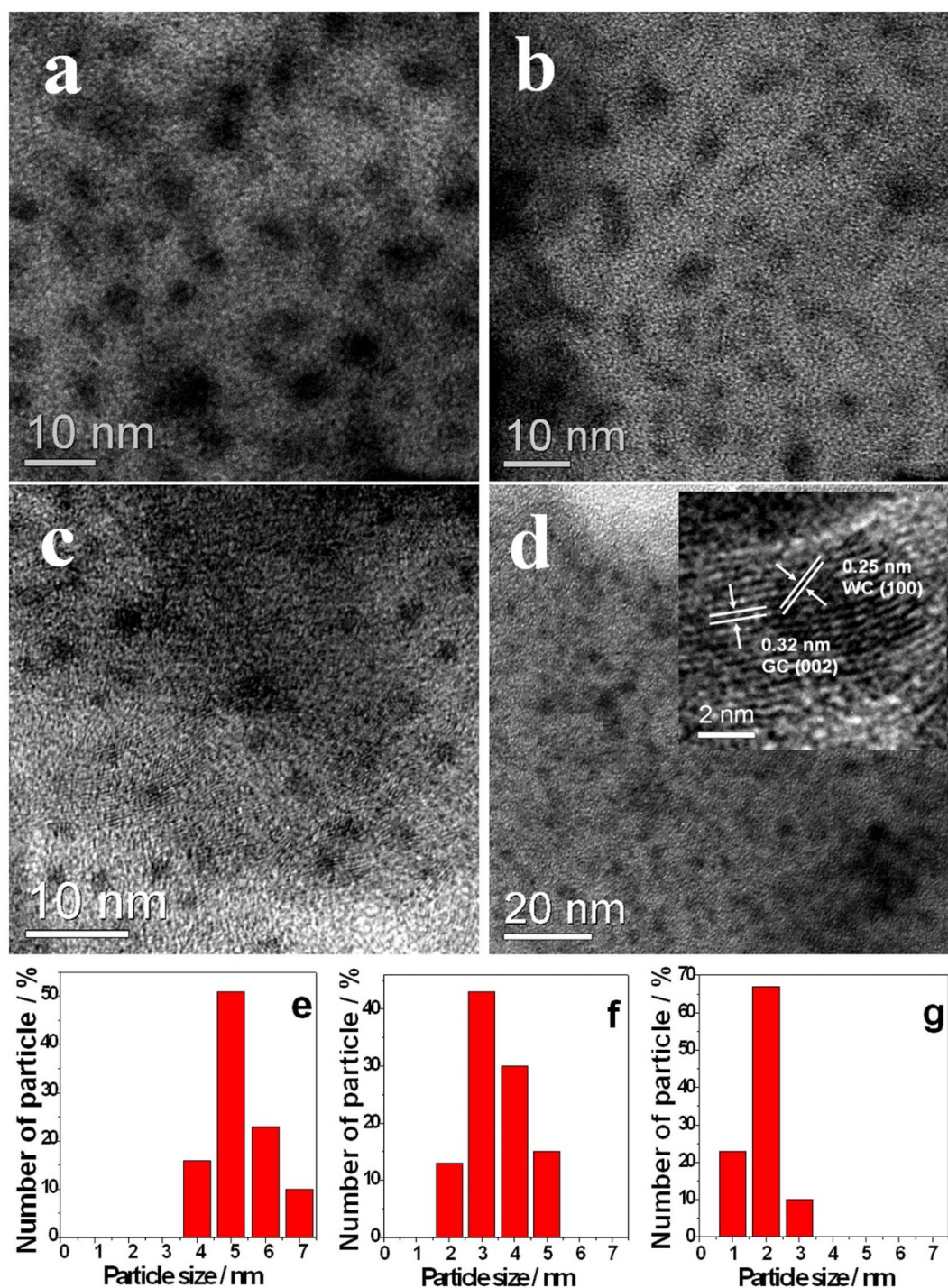


**Figure 3** | TEM images and histograms of (a) WC-GC10, (b) WC-GC5 and (c) WC-GC2. (a)–(c) TEM images of the samples heated at 650°C for 3 h, (d) TEM image of the WC-GC5 sample with small magnification, inset is the HRTEM image and (e)–(g) the histograms of the WC particles.

To further understand the effect of iron on the formation of WC, the effect of the Fe/W atom molar ratio was also evaluated. The results as shown above were obtained in a solution with excess  $K_4[Fe(CN)_6]$  ( $0.05 \text{ mol L}^{-1}$ ) compared with AMT. The product is totally different if less  $K_4[Fe(CN)_6]$  used. Figure S1 shows the XRD patterns of the resin exchanged in 10 times lower concentration of  $0.005 \text{ mol L}^{-1} K_4[Fe(CN)_6]$  and higher concentration of  $0.0014 \text{ mol L}^{-1}$  AMT (W atom concentration is  $0.01 \text{ mol L}^{-1}$ ) which was heated at different temperatures. The ratio of the Fe to W was 1:2. It can be found in Figure S1 that  $FeWO_4$  can form at 650°C. However, the final product was a mixture of WC and  $W_2C$ . The reason is that part of the

WC formed via the direct conversion of  $FeWO_4 \rightarrow WC$  and part of the WC was produced via the pathway of  $WO_2 \rightarrow WC_{1-x} \rightarrow W_2C \rightarrow WC$ . According to the formula of  $FeWO_4$ , the atomic ratio of Fe to W is 1:1. The excess W can only be converted to WC via other reaction mechanism as shown in equation (6). In that case, the product is a mixture of carbides even higher temperature is used.

In conclusion, the pure WC can be readily formed at lower temperatures in the presence of iron precursor with the excess of Fe to W captured by ion exchange with resin. The development of an energy-saving method for synthesizing nanosized WC at ultralow temperature and short processing time is of significance for practical

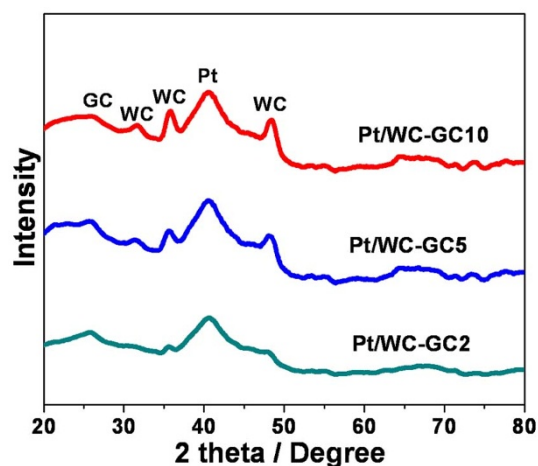


Figure 4 | XRD patterns of Pt/WC-GC10, Pt/WC-GC5 and Pt/WC-GC2.

application. We tried to further reduce the temperature and proved that WC could be formed at the temperature of as lower as 580°C. Figure S2a shows the XRD patterns of WC-GC2, WC-GC5 and WC-GC10 heat treated at 580°C for 20 h. The results were similar with that shown in Figure 1. Only WC with iron compounds was found. After the treatment of the sample in 5 M HCl solution, all the iron compounds were removed as shown in Figure S2b. It revealed that WC not only can be synthesized at very low temperature in an iron-containing system but also is stable in an acidic solution.

Figure S3 shows the XRD patterns of WC-GC2, WC-GC5 and WC-GC10 heated at 650°C and 800°C. They all have graphite (GC), WC, Fe<sub>2</sub>C and Fe<sub>3</sub>C peaks but no peaks of other W compounds or W metal, indicating 100% yield of WC was achieved through this energy and time efficient synthesis route.

The Raman spectroscopic measurements further proved that the resin was partially graphitized under the catalysis of iron (Figure S3c). The ratios of the G-line to D-line were used to judge the degree of the graphitization. The G-line at 1585 cm<sup>-1</sup> corresponds to a splitting of the E<sub>2g</sub> stretching mode of graphite and reflects the structural intensity of the sp<sup>2</sup>-hybridized carbon atom<sup>60,61</sup>. The D-line at 1350 cm<sup>-1</sup> is attributed to the vibrations of carbon atoms with dangling bonds in disordered graphite planes and the defects incorporated into pentagon and heptagon graphite-like structures. The I<sub>G</sub>/I<sub>D</sub> values for WC-GC2, WC-GC5 and WC-GC10 were 1.52, 1.39 and 1.36, respectively. The results show that the samples prepared in

Table 1 | The performance comparison of the four electrocatalysts

Electrocatalyst	Pt mass content*	<i>i</i> <sub>m</sub> at 0.9 V (mA mg <sup>-1</sup> Pt)
Pt/WC-GC10	37.5%	213.8
Pt/WC-GC5	37.9%	257.7
Pt/WC-GC2	37.8%	191.8
Pt/C	47.6%	124.6

\*The data were determined by inductively coupled plasma-atomic emission spectrometry (icp).

dilute AMT concentration gave a higher degree of graphitization. This is reasonable since the concentration of iron precursor was maintained the same but the concentration of tungsten precursor was reduced.

Figure S3d shows the typical TG and DTG results of the sample after ion-exchanged in 0.05 mol L<sup>-1</sup> K<sub>4</sub>[Fe(CN)<sub>6</sub>] and 0.0007 mol L<sup>-1</sup> AMT solution (atom concentration of W is 0.005 mol L<sup>-1</sup>) in N<sub>2</sub> atmosphere. The mass loss before 80°C is the evaporation of free water moisture. The sharp mass loss between 300 and 450°C corresponds to the evaporation and decomposition of the resin with releasing of CO, CO<sub>2</sub>. The slow mass loss after 500°C corresponds to a continuous process of carbonization and graphitization of the melted resin along with the formation of WC nanoparticles. The DTG curve reached zero after 3 h at 650°C means all W was converted to the stable WC nanoparticles.

The results in Figure S2 and Figure S3 proved our theory in reaction mechanism. The final products maintain almost the same in structure after 20 hours heating at 580°C, 3 hours heating at 650°C and directly heated to 800°C without temperature holding. This indicates that the FeWO<sub>4</sub> can be converted to WC at a temperature of as low as 580°C, however, the conversion rate is temperature dependent with higher temperature results in higher conversion rate.

In summary, the WC nanoparticles as small as less than 2 nm on graphitized carbon were effectively synthesized for the first time at a significantly lower temperature compared to conventional method. Furthermore, a new reaction mechanism is proposed which involves the conversion of FeWO<sub>4</sub> to form the nanoscale WC. This formation pathway is based on an ion-exchange resin as carbon source to locally anchor the W source and Fe source as graphitization catalyst. With a proper recipe, FeWO<sub>4</sub> as an intermediate can be formed at lower temperature which can then be directly converted into WC along with the carbonization of resin without the coexistence of other tungsten compounds and metal W in the final product. The dispersion of W and Fe are uniform due to the natural of ion exchange

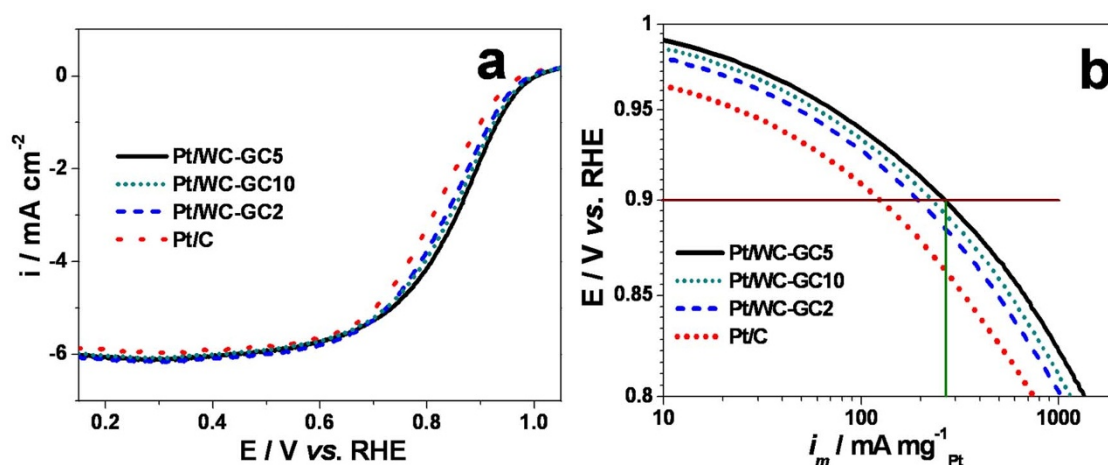


Figure 5 | (a) Polarization curves on Pt/WC-GC10, Pt/WC-GC5, Pt/WC-GC2 and commercial Pt/C electrodes in O<sub>2</sub> saturated 0.1 mol L<sup>-1</sup> HClO<sub>4</sub> solution, 25°C, scan rate: 5 mV s<sup>-1</sup>, 1600 rpm and (b) the corresponding mass activities by mass-transport correction.



Table 2 | WC mass contents in WC-GC samples

Sample	WC-GC2	WC-GC5	WC-GC10
WC content/wt%	9.7	17.8	50.6

process, which is beneficial to the formation of  $\text{FeWO}_4$  and the conversion into WC. This finding opens an energy-saving route to mass produce nanoscale WC with extremely high yield. It is possible to apply this mechanism to synthesize other nanosized carbides.

The nanosized WC on graphitized carbon showed highly enhanced electrocatalytic activity for oxygen reduction reaction after the loading of Pt nanoparticles. The result indicated that the Pt nanoparticles deposited on WC-GC dominated by Pt (111) plane, which has been approved to be the most active site for ORR. A typical electrocatalyst, Pt/WC-GC5, showed mass activity of as high as  $257.7 \text{ mA mg}^{-1}_{\text{Pt}}$  @  $0.9 \text{ V}$  which is two times higher than that of commercial Pt/C electrocatalyst.

## Methods

**Synthesis. Preparation of WC-GC with ion-exchange resin as carbon source.** The mixtures of solutions with three different concentrations of ammonium metatungstate (AMT, A.R. Tianjin Jinke Fine Chemicals, China) and  $\text{K}_4[\text{Fe}(\text{CN})_6]$  (A.R. Guangzhou Chemical Reagent Factory, China) in deionized water (100 ml) was equally prepared. The polyacrylic weak-base anion-exchange resin (D314, 10 g, Shanghai Hualing Resin Co., Ltd, China) was then impregnated into these three solutions and followed by washing with D.I. water for 3 times, respectively. The exchanged resin was further dried and heated at different temperatures in  $\text{N}_2$  atmosphere. The final WC-GC samples were grinded and treated with  $5 \text{ mol L}^{-1}$  HCl solution to remove the Fe element. The WC-GC samples prepared with  $\text{K}_4[\text{Fe}(\text{CN})_6]$  concentration of  $0.05 \text{ mol L}^{-1}$  and AMT concentrations of  $0.0014$ ,  $0.0007$  and  $0.0003 \text{ mol L}^{-1}$  (W atom concentrations were  $0.01$ ,  $0.005$  and  $0.002 \text{ mol L}^{-1}$ ) were denoted as WC-GC10, WC-GC5 and WC-GC2, respectively. The samples without  $\text{K}_4[\text{Fe}(\text{CN})_6]$  were also prepared with the same process.

**Preparation of Pt/WC-GC electrocatalyst.** Pt supported on the WC-GC10, WC-GC5 and WC-GC2 (denoted as Pt/WC-GC10, Pt/WC-GC5 and Pt/WC-GC2) samples were prepared and evaluated for oxygen reduction reaction. Typically, WC-GC (50 mg) were added to a mixture of  $45.46 \text{ mg H}_2\text{PtCl}_6$  and  $20 \text{ ml glycol}$  (A.R. Tianjin Fuyu Fine Chemicals Co., Ltd, China) to form an uniform ink in ultrasonic bath for 30 min. The pH of the mixture was then adjusted to 10 by adding  $5 \text{ wt\% NaOH/glycol}$  solution (A.R. Guangzhou Chemical Reagent Factory, China) and put into a homemade programmable microwave oven (1000W, 2.45 GHz) for heating at a 5 s on and 5 s off procedure for 20 times. Afterwards, the mixture was washed with water for 4–5 times and dried in vacuum at  $80^\circ\text{C}$  for 2 h. The Pt contents in the electrocatalyst were targeted as 40 wt%. The actual Pt contents were determined by Inductively Coupled Plasma-atomic Emission Spectrometry (ICP, IRIS(HR), USA) method.

**Characterizations.** 5 mg Pt/WC-GC or 4 mg Pt/C (47.6 wt% Pt) were dispersed in 1.95 ml ethanol and 0.05 ml 5 wt% Nafion suspension (DuPont, USA) under ultrasonic agitation to form the electrocatalyst ink. The electrocatalyst ink (2.5  $\mu\text{l}$ ) was deposited on the surface of a grassy carbon rotating disk electrode and dried at room temperature. The total Pt loadings were  $0.01 \text{ mg cm}^{-2}$ . The electrochemical measurements were carried out in an oxygen-saturated  $0.1 \text{ mol L}^{-1} \text{ HClO}_4$  (A.R. Guangdong Guanghua Chemical Co., Ltd) solution scanned between 0 to 1.1 V at a scan rate of  $5 \text{ mV s}^{-1}$  at  $25^\circ\text{C}$ . A platinum foil ( $1.0 \text{ cm}^2$ ) and a reversible hydrogen electrode (RHE) were used as counter and reference electrodes, respectively.

All chemicals were purchased as analytical grade and used as received.

The morphologies of the WC-GC and electrocatalysts were characterized by transmission electron microscopy (TEM, JOEP JEM-2010, JEOL Ltd.) operating at 200 kV. The crystal structures of the prepared samples were determined using a X-ray diffractometer (D/Max-III A, Rigaku Co., Japan,  $\text{CuK}\alpha$ ,  $\lambda = 1.54056 \text{ \AA}$  radiation), the graphitization degrees of WC-GC were determined with Laser Micro-Raman Spectrometer (Renishaw inVia, Renishaw plc). The mass change with temperature and time were determined by a thermogravimetry coupled with Fourier transform infrared spectrometer (TG-IR, TG-209/Vector-22).

- Kumar, A., Singh, K. & Pandey, O. P. Sintering behavior of nanostructured WC-Co composite. *Ceram. Int.* **37**, 1415–1422 (2011).
- Feng, K., Xiong, J., Sun, L., Fan, H. & Zhou, X. The process of combustion synthesis of WC-Co composites under the action of an electric field. *J. Alloy. Compd.* **504**, 277–283 (2010).
- Huang, B., Chen, L. D. & Bais, Q. Bulk ultrafine binderless WC prepared by spark plasma sintering. *Scripta Mater.* **54**, 441–445 (2006).

- Rodiger, K., Dreyer, K., Gerdes, T. & Willert-Porada, M. Microwave sintering of hardmetals. *Int. J. Refract. Met. H.* **16**, 409–416 (1998).
- Kim, H. C., Jeong, I. K., Shon, I. J., Ko, I. Y. & Do, J. Fabrication of WC-8 wt.% Co hard materials by two rapid sintering processes. *Int. J. Refract. Met. H.* **25**, 336–340 (2007).
- Azcona, I., Ordóñez, A., Sánchez, J. M. & Castro, F. Hot isostatic pressing of ultrafine tungsten carbide-cobalt hardmetals. *J. Mater. Sci.* **37**, 4189–4195 (2002).
- Stefaniak, A. B., Virji, M. A. & Day, G. A. Characterization of exposures among cemented tungsten carbide workers. Part I: size-fractionated exposures to airborne cobalt and tungsten particles. (Report). *J. Expo. Sci. Env. Epid.* **19**, 475–491 (2009).
- Kear, B. H. & Mc Candlish, L. E. Chemical processing and properties of nanostructured WC-Co Materials. *Nanostruct. Mater.* **3**, 19–30 (1993).
- Goren-Muginstein, G. R., Berger, S. & Rosen, A. Sintering study of nanocrystalline tungsten carbide powders. *Nanostruct. Mater.* **10**, 795–804 (1998).
- Levy, R. L. & Boudart, M. Platinum-like behavior of tungsten carbide in surface catalysis. *Science* **181**, 547–549 (1973).
- Santos, J. B. O., Valen, G. P. & Rodrigues, J. A. J. Catalytic decomposition of hydrazine on tungsten carbide: the influence of adsorbed oxygen. *J. Catal.* **210**, 1–6 (2002).
- Moreno-Castilla, C., Alvarez-Merino, M. A., Carrasco-Marín, F. & Fierro, J. L. G. Tungsten and tungsten carbide supported on activated carbon: Surface structures and performance for ethylene hydrogenation. *Langmuir* **17**, 1752–1756 (2001).
- Patrick, C. D., Jean, L. L. & Claude, P. Tetralin hydrogenation catalyzed by  $\text{Mo}_2\text{C}/\text{Al}_2\text{O}_3$  and  $\text{WC}/\text{Al}_2\text{O}_3$  in the presence of  $\text{H}_2\text{S}$ . *Catal. Today* **65**, 195–200 (2001).
- Pang, J., Zheng, M., Wang, A. & Zhang, T. Catalytic hydrogenation of corn stalk to ethylene glycol and 1,2-propylene glycol. *Ind. Eng. Chem. Res.* **50**, 6601–6608 (2011).
- Ji, N. *et al.* Cover picture: direct catalytic conversion of cellulose into ethylene glycol using nickel-promoted tungsten carbide catalysts. *Angew. Chem. Int. Ed.* **47**, 8510–8513 (2008).
- Iyer, M. V., Norcio, L. P., Kugler, E. L. & Dadyburjor, D. B. Kinetic modeling for methane reforming with carbon dioxide over a mixed-metal carbide catalyst. *Ind. Eng. Chem. Res.* **42**, 2712–2721 (2003).
- Hwu, H. H., Chen, J. G. & Kourtakas, K. Potential application of tungsten carbides as electrocatalysts. I. decomposition of methanol over carbide-modified W(111). *J. Phys. Chem. B* **105**, 10037–10044 (2001).
- Neylon, M. K., Choi, S. & Kwon, H. Catalytic properties of early transition metal nitrides and carbides: n-butane hydrogenolysis, dehydrogenation and isomerization. *Appl. Catal. A* **183**, 253–263 (1999).
- Delannoy, L., Giraudon, J. M. & Granger, P. Group VI transition metal carbides as alternatives in the hydrodechlorination of chlorofluorocarbons. *Catal. Today* **59**, 231–240 (2000).
- Keller, V., Wehrer, P., Garin, F., Ducros, R. & Maire, G. Catalytic activity of bulk tungsten carbides for alkane reforming: I. Characterization and catalytic activity for reforming of hexane isomers in the absence of oxygen. *J. Catal.* **153**, 9–16 (1995).
- Keller, V., Wehrer, P., Garin, F., Ducros, R. & Maire, G. Catalytic activity of bulk tungsten carbides for alkane reforming. II. Catalytic activity of tungsten carbides modified by oxygen. *J. Catal.* **166**, 125–135 (1997).
- Meng, H. *et al.* Selective cathode catalysts for mixed-reactant alkaline alcohol fuel cells. *Fuel Cells* **6**, 447–450 (2006).
- Philip, N. R. & Paul, S. The relation of surface structure to the electrocatalytic activity of tungsten carbide. *J. Catal.* **48**, 42–59 (1977).
- Miles, R. The characterization and evaluation of highly dispersed tungsten carbide electrocatalysts. *J. Chem. Tech. Biotechnol.* **30**, 35–43 (1980).
- Burstein, G. T., Barnett, C. J. & Kucernak, A. R. J. Anodic oxidation of methanol using a new base electrocatalyst. *J. Electrochem. Soc.* **143**, 139–140 (1996).
- Nakazawa, M. & Okamoto, H. Surface composition of prepared tungsten carbide and its catalytic activity. *Appl. Surf. Sci.* **24**, 75–86 (1985).
- Liu, Y. & Mustain, W. E. Structural and electrochemical studies of Pt clusters supported on high-surface-area tungsten carbide for oxygen reduction. *ACS Catal.* **1**, 212–220 (2011).
- Yan, Z. X. *et al.* A facile route to carbide-based electrocatalytic nanocomposites. *J. Mater. Chem.* **22**, 5072–5079 (2012).
- Hsu, I. J., Kimmel, Y. C., Dai, Y., Chen, S. & Chen, J. G. Rotating disk electrode measurements of activity and stability of monolayer Pt on tungsten carbide disks for oxygen reduction reaction. *J. Power Sources* **199**, 46–52 (2012).
- Shao, M. *et al.* Tungsten carbide modified high surface area carbon as fuel cell catalyst support. *J. Power Sources* **196**, 7426–7434 (2011).
- Lee, Y. W., Ko, A. R., Han, S. B., Kim, H. S. & Park, K. W. Synthesis of octahedral Pt-Pd alloy nanoparticles for improved catalytic activity and stability in methanol electrooxidation. *Phys. Chem. Chem. Phys.* **13**, 5569–5572 (2011).
- Wang, R. H. *et al.* Small-sized and contacting Pt-WC nanostructures on graphene as highly efficient anode catalysts for direct methanol fuel cells. *Chem-Eur. J.* **18**, 7443–7451 (2012).
- Hu, F., Cui, G., Wei, Z. & Shen, P. K. Improved kinetics of ethanol oxidation on Pd catalysts supported on tungsten carbides/carbon nanotubes. *Electrochem. Commun.* **10**, 1303–1306 (2008).



34. Zhao, Z. *et al.* The origin of the high performance of tungsten carbides/carbon nanotubes supported Pt catalysts for methanol electrooxidation. *Electrochem. Commun.* **11**, 290–293 (2009).
35. Ganesan, R., Ham, D. J. & Lee, J. S. Platinized mesoporous tungsten carbide for electrochemical methanol oxidation. *Electrochem. Commun.* **9**, 2576–2579 (2007).
36. Lu, J. L., Li, Z. H., Jiang, S. P., Shen, P. K. & Li, L. Nanostructured tungsten carbide/carbon composite synthesized by a microwave heating method as supports of platinum catalysts for methanol oxidation. *J. Power Sources* **202**, 56–62 (2012).
37. Meng, H. & Shen, P. K. The beneficial effect of the addition of tungsten carbides to Pt catalysts on the oxygen electroreduction. *Chem. Commun.* **35**, 4408–4410 (2005).
38. Meng, H. & Shen, P. K. Tungsten carbides nanocrystals promoted Pt/C electrocatalysts for oxygen reduction. *J. Phys. Chem. B* **109**, 22705–22709 (2005).
39. Binder, H., Köhling, A., Kuhn, W., Lindner, W. & Sandstede, G. Tungsten carbide electrodes for fuel cells with acid electrolyte. *Nature* **224**, 1299–1300 (1969).
40. Bosco, J. P., Sasaki, K., Sadakane, M., Ueda, W. & Chen, J. G. Synthesis and characterization of three-dimensionally ordered macroporous (3DOM) tungsten carbide: Application to direct methanol fuel cells. *Chem. Mater.* **3**, 966–973 (2010).
41. Pol, V. G., Pol, S. V. & Gedanken, A. Dry autoclaving for the nanofabrication of sulfides, selenides, borides, phosphides, nitrides, carbides, and oxides. *Adv. Mater.* **23**, 1179–1190 (2011).
42. McIntyre, D. R., Burstein, G. T. & Vossen, A. Effect of carbon monoxide on the electrooxidation of hydrogen by tungsten carbide. *J. Power Sources* **107**, 67–73 (2002).
43. Yan, Y. *et al.* Template-free pseudomorphic synthesis of tungsten carbide nanorods. *Small* **8**, 3350–3356 (2012).
44. Shen, P. K., Yin, S., Li, Z. & Chen, C. Preparation and performance of nanosized tungsten carbides for electrocatalysis. *Electrochim. Acta* **55**, 7969–7974 (2010).
45. Lee, J. D., Lee, D. H., Park, N. K., Ryu, S. O. & Lee, T. J. The preparation of nanophase tungsten carbide powder with zeolite-X catalysts. *Appl. Phys.* **6**, 1040–1043 (2006).
46. Wang, Y., Song, S. Q., Maragou, V., Shen, P. K. & Tsiakaras, P. High surface area tungsten carbide microspheres as effective Pt catalyst support for oxygen reduction reaction. *Appl. Catal.* **89**, 223–228 (2009).
47. Cui, G. F., Shen, P. K., Meng, H., Zhao, J. & Wu, G. Tungsten carbide as supports for Pt electrocatalysts with improved CO tolerance in methanol oxidation. *J. Power Sources* **196**, 6125–6130 (2011).
48. Hu, L., Ji, S., Jiang, Z., Song, H., Wu, P. & Liu, Q. Direct synthesis and structural characteristics of ordered SBA-15 mesoporous silica containing tungsten oxides and tungsten carbides. *J. Phys. Chem. C* **111**, 15173–15184 (2007).
49. Wu, Z. *et al.* Silica-templated synthesis of ordered mesoporous tungsten carbide/graphitic carbon composites with nanocrystalline walls and high surface areas via a temperature-programmed carburization route. *Small* **5**, 2738–2749 (2009).
50. Pol, V. G., Pol, S. V. & Gedanken, A. One-step synthesis and characterization of SiC, Mo<sub>2</sub>C, and WC nanostructures. *Eur. J. Inorg. Chem.* 709–715 (2009).
51. Reddy, K. M., Rao, T. N., Radha, K. & Joardar, J. Nanostructured tungsten carbides by thermochemical processing. *J. Alloy. Compd.* **494**, 404–409 (2010).
52. Moustafa, S. F., Abdel-Hamid, Z., Baheig, O. G. & Hussien, A. Synthesis of WC hard materials using coated powders. *Adv. Powder. Technol.* **22**, 596–601 (2011).
53. Nelson, J. A. & Wagner, M. J. High surface area Mo<sub>2</sub>C and WC prepared by alkalide reduction. *Chem. Mater.* **14**, 1639–1642 (2002).
54. Oxley, J. D., Mdleleni, M. M. & Suslick, K. S. Hydrodehalogenation with sonochemically prepared Mo<sub>2</sub>C and W<sub>2</sub>C. *Catal. Today* **88**, 139–151 (2004).
55. Kim, J. C. & Kim, B. K. Synthesis of nanosized tungsten carbide powder by the chemical vapor condensation process. *Scripta. Mater.* **50**, 969–972 (2004).
56. Palmquist, J. P. *et al.* Magnetron sputtered W-C films with C60 as carbon source. *Thin Solid Films* **444**, 29–37 (2003).
57. Pol, S. V., Pol, V. G. & Gedanken, A. Synthesis of WC nanotubes. *Adv. Mater.* **18**, 2023–2027 (2006).
58. Zhu, Q., Zhou, S., Wang, X. & Dai, S. Controlled synthesis of mesoporous carbon modified by tungsten carbides as an improved electrocatalyst support for the oxygen reduction reaction. *J. Power Sources* **193**, 495–500 (2009).
59. Chouzier, S., Afanasiev, P., Vrinat, M., Cseri, T. & Roy-Auberger, M. One-step synthesis of dispersed bimetallic carbides and nitrides from transition metals hexamethylenetetramine complexes. *J. Solid State Chem.* **179**, 3314–3123 (2006).
60. Dresselhaus, M. S., Dresselhaus, G. & Saito, R. A Raman spectroscopy of carbon nanotubes. *A. Jorio, Phys. Rep.* **409**, 47–99 (2005).
61. Belin, T. & Epron, F. Characterization methods of carbon nanotubes: A review. *Mater. Sci. Eng. B* **119**, 105–118 (2005).
62. Lim, B. *et al.* Pd-Pt bimetallic nanodendrites with high activity for oxygen reduction. *Science* **324**, 1302–1305 (2009).
63. Gasteiger, H. A., Kocha, S. S., Sompalli, B. & Wagner, F. T. Activity benchmarks and requirements for Pt, Pt-alloy, and non-Pt oxygen reduction catalysts for PEMFCs. *Appl. Catal. B* **56**, 9–35 (2005).

## Acknowledgements

This work was supported by the link project of the National Natural Science Foundation of China and Guangdong Province (U1034003), the National Natural Science Foundation of China (21073241), the Major International (Regional) Joint Research Project (51210002) and General Motors (Project No. RD-07-295-NV508).

## Author contributions

Z.X.Y. carried out experiments, analyzed and discussed data and wrote the paper; M.C. discussed, analyzed data and wrote the paper; P.K.S. conceived, designed and carried out experiments, analyzed and discussed data and wrote the paper.

## Additional information

Supplementary information accompanies this paper at <http://www.nature.com/scientificreports>

**Competing financial interests:** The authors declare no competing financial interests.

**License:** This work is licensed under a Creative Commons Attribution-NonCommercial-NoDerivs 3.0 Unported License. To view a copy of this license, visit <http://creativecommons.org/licenses/by-nc-nd/3.0/>

**How to cite this article:** Yan, Z.X., Cai, M. & Shen, P.K. Nanosized tungsten carbide synthesized by a novel route at low temperature for high performance electrocatalysis. *Sci. Rep.* **3**, 1646; DOI:10.1038/srep01646 (2013).